

**DEVELOPMENT OF TITANIUM DIOXIDE  
NANOPARTICLES/NANOSOLUTION FOR PHOTOCATALYTIC  
ACTIVITY**

**by**

**SITI AIDA BINTI IBRAHIM**

**Thesis submitted in fulfilment of the  
requirements for the degree of  
Doctor of Philosophy**

**JUNE 2015**

## ACKNOWLEDGEMENTS

Firstly, I would like to express my deepest gratitude to my supervisor Assoc. Prof. Dr. Ir. Srimala Sreekantan for her expert guidance, constant attention, valuable suggestions, enthusiastic support and personal concern during the research and through the course of my study. Her fruitful ideas throughout the research project has helped me accomplished this work successfully.

Special thanks to the Dean of School of Material and Mineral Resources Engineering, Professor Hanafi Ismail for his permission to let me use all the brilliant facilities and equipment in completing my project. Under his leadership, he has created a healthy learning environment in the school. I would also like to extend my sincere appreciation to thank the technical staffs of School of Materials and Mineral Resources Engineering, especially to Mdm. Fong Lee Lee, Mrs Haslina, Mr. Azrul, and Mr. Zulkurnain for their various contributions in one way or another.

To my dear friends and labmates, Norwanis, , Suhaina, Khairul Arifah, Nur Hidayati, Syahriza and all close members of postgraduate room of School of Materials and Mineral Resources Engineering, thank you for making my life in USM so colourful and enjoyable. Last, but not least to my family especially to my ever-loving mother whom are always on my side, Hajjah Rinah Binti Mohd. Jirin, Thank you for the support and the encouragement you gave me to pursue my dreams. Not to forget, my family members who always be there for me through my thick and thin.

Siti Aida Ibrahim

June 2015

## TABLE OF CONTENTS

|   |       |
|---|-------|
| ACKNOWLEDGEMENTS.....                   | ii    |
| TABLE OF CONTENTS.....                  | iii   |
| LIST OF FIGURES.....                    | ix    |
| LIST OF TABLES.....                     | xv    |
| LIST OF ABBREVIATIONS.....              | xviii |
| LIST OF SYMBOLS.....                    | xx    |
| LIST OF PUBLICATIONS & AWARDS.....      | xxi   |
| ABSTRAK.....                            | xxii  |
| ABSTRACT.....                           | xxiv  |
| <br>                                    |       |
| CHAPTER 1 – INTRODUCTION.....           | 1     |
| 1.1 Introduction.....                   | 1     |
| 1.2 Problem Statement.....              | 4     |
| 1.3 Objectives.....                     | 8     |
| 1.4 Scope of work.....                  | 9     |
| 1.5 Thesis overview.....                | 9     |
| <br>                                    |       |
| CHAPTER 2 - LITERATURE REVIEW.....      | 11    |
| 2.1 Introduction.....                   | 11    |
| 2.2 TiO <sub>2</sub> nanoparticles..... | 13    |
| 2.3 Historical overview.....            | 15    |
| 2.4 Principle of the photocatalyst..... | 19    |
| 2.5 Factors that affecting PCA.....     | 21    |

|         |  |    |
|---------|--|----|
| 2.5.1   | Particle size.....   | 21 |
| 2.5.2   | Phase structure.....   | 23 |
| 2.5.3   | TiO <sub>2</sub> dosage.....                                   | 23 |
| 2.6     | TiO <sub>2</sub> synthesis.....                                | 24 |
| 2.6.1   | Sonochemical method.....                                       | 25 |
| 2.6.2   | Vapor deposition (VD).....                                     | 25 |
| 2.6.3   | Sol-gel method.....  | 27 |
| 2.7     | Factor that affecting sol-gel process.....                     | 32 |
| 2.7.1   | pH of hydrolysis medium.....                                   | 32 |
| 2.7.2   | Post- heat treatment.....                                      | 33 |
| 2.7.2.1 | Annealing.....   | 33 |
| 2.7.2.2 | Hydrothermal treatment.....                                    | 34 |
| 2.7.2.3 | Peptization.....   | 36 |
| 2.8     | Modification of TiO <sub>2</sub> to Harvest Visible Light..... | 38 |
| 2.8.1   | Anion incorporation.....                                       | 39 |
| 2.8.2   | Cation incorporation.....                                      | 40 |
| 2.8.2.1 | Noble metal.....   | 41 |
| 2.8.2.2 | Transition metal.....  | 45 |
| 2.8.2.3 | Rare earth metal.....  | 50 |
| 2.9     | Photocatalyst functionality.....                               | 59 |
| 2.9.1   | Water treatment with TiO <sub>2</sub> .....                    | 59 |
| 2.9.2   | Air Quality improvement with TiO <sub>2</sub> .....            | 60 |
| 2.9.3   | Antibacterial effect of TiO <sub>2</sub> .....                 | 63 |
| 2.10    | Reviews and drawbacks of existing technology.....              | 66 |

|  |    |
|--|----|
| CHAPTER 3 - METHODOLOGY.....                                     | 69 |
| 3.1 Introduction.....  | 69 |
| 3.2 Raw materials and apparatus.....                             | 69 |
| 3.3 TiO <sub>2</sub> nanoparticles.....                          | 70 |
| 3.4 Synthesis of TiO <sub>2</sub> .....                          | 72 |
| 3.4.1 Heat treatment process.....                                | 72 |
| 3.4.2 Annealing.....   | 72 |
| 3.4.3 Hydrothermal treatment.....                                | 73 |
| 3.4.4 Peptization.....   | 74 |
| 3.5 Synthesis of Fe-TiO <sub>2</sub> .....                       | 74 |
| 3.6 Synthesis of Ag-TiO <sub>2</sub> .....                       | 74 |
| 3.7 Synthesis of Zr-TiO <sub>2</sub> .....                       | 75 |
| 3.8 Synthesis of Ag-Zr-TiO <sub>2</sub> .....                    | 75 |
| 3.9 Experimental design.....                                     | 75 |
| 3.9.1 Effect of water to Ti ratio.....                           | 76 |
| 3.9.2 Effect of pH.....  | 77 |
| 3.9.3 Effect of annealing in different atmosphere condition..... | 78 |
| 3.9.4 Effect of cation incorporation.....                        | 78 |
| 3.10 Functionality studies.....                                  | 80 |
| 3.10.1 Methyl orange degradation.....                            | 81 |
| 3.10.2 Antibacterial activity.....                               | 82 |
| 3.10.2.1 Disc/Cotton Diffusion assay.....                        | 82 |
| 3.10.2.2 Swab test.....  | 82 |
| 3.10.3 Field work Study.....                                     | 83 |
| 3.10.3.1 Antibacterial monitoring.....                           | 84 |

|   |   |     |
|---|---|-----|
| 3.10.3.2                                | VOC Detoxifying.....                                  | 84  |
| 3.11                                    | Characterization.....                                 | 86  |
| 3.11.1                                  | XRD.....  | 86  |
| 3.11.2                                  | FESEM & EDX.....                                      | 87  |
| 3.11.3                                  | TEM.....  | 88  |
| 3.11.4                                  | BET.....  | 89  |
| 3.11.5                                  | Ultraviolet-Visible Spectrophotometer .....           | 90  |
| 3.11.6                                  | Zetasizer Nano Series Machine.....                    | 91  |
| 3.11.7                                  | Fourier Transmission Infra-red.....                   | 91  |
| 3.11.8                                  | Photoluminescence Spectroscopy.....                   | 92  |
| CHAPTER 4 - RESULTS AND DISCUSSION..... |   | 93  |
| 4.1                                     | Introduction.....                                     | 93  |
| 4.2                                     | Synthesis of pure TiO <sub>2</sub> nanoparticles..... | 93  |
| 4.2.1                                   | Effect of water to Ti ratio.....                      | 94  |
| 4.2.2                                   | Effect of heat treatment.....                         | 98  |
| 4.2.2.1                                 | Annealing.....  | 98  |
| 4.2.2.2                                 | Effect of pH.....                                     | 104 |
| 4.2.2.3                                 | Effect of annealing in different atmosphere condition | 116 |
| 4.2.3                                   | TiO <sub>2</sub> via hydrothermal method.....         | 123 |
| 4.2.4                                   | TiO <sub>2</sub> via peptization process.....         | 130 |
| 4.2.5                                   | PCA with different catalyst loading.....              | 136 |
| 4.2.6                                   | MO degradation under UV and visible light.....        | 137 |
| 4.3                                     | Cation TiO <sub>2</sub> Synthesis.....                | 138 |
| 4.3.1                                   | Synthesis of Fe-TiO <sub>2</sub> nanoparticles.....   | 139 |

|         |  |     |
|---------|--|-----|
| 4.3.1.1 | Fe-TiO <sub>2</sub> via hydrothermal treatment.....    | 139 |
| 4.3.1.2 | Fe-TiO <sub>2</sub> via peptization process.....       | 145 |
| 4.3.1.3 | PCA of Fe-TiO <sub>2</sub> under UV.....               | 149 |
| 4.3.1.4 | PCA of Fe-TiO <sub>2</sub> under visible light.....    | 150 |
| 4.3.2   | Synthesis of Ag-TiO <sub>2</sub> .....                 | 152 |
| 4.3.2.1 | PCA of Ag-TiO <sub>2</sub> under visible light.....    | 157 |
| 4.3.2.2 | Antibacterial activity of Ag-TiO <sub>2</sub> .....    | 161 |
| 4.3.3   | Synthesis of Zr-TiO <sub>2</sub> .....                 | 165 |
| 4.3.3.1 | Effect of Zr addition method.....                      | 165 |
| 4.3.3.2 | Effect of Zr concentration.....                        | 166 |
| 4.3.3.3 | PCA of Zr-TiO <sub>2</sub> under visible light.....    | 170 |
| 4.3.3.4 | Antibacterial activity of Zr-TiO <sub>2</sub> .....    | 172 |
| 4.3.4   | Synthesis of Ag-Zr-TiO <sub>2</sub> .....              | 173 |
| 4.3.4.1 | PCA of Ag-Zr-TiO <sub>2</sub> .....                    | 179 |
| 4.3.4.2 | Antibacterial activity of Ag-Zr-TiO <sub>2</sub> ..... | 182 |
| 4.3.5   | Comparison with commercial product.....                | 184 |
| 4.3.5.1 | Morphology analysis.....                               | 184 |
| 4.3.5.2 | Crystal structure analysis.....                        | 185 |
| 4.3.5.3 | Light absorption characteristic.....                   | 185 |
| 4.3.5.4 | PCA.....   | 186 |
| 4.3.5.5 | Antibacterial Study via Diffusion Method.....          | 187 |
| 4.3.5.6 | Antibacterial study via Swab test.....                 | 188 |
| 4.4     | Field work study.....                                  | 190 |
| 4.4.1   | Antibacterial monitoring.....                          | 190 |
| 4.4.2   | VOC detoxification.....                                | 191 |

|  |     |
|--|-----|
| CHAPTER 5 - CONCLUSION AND FURTHER WORK..... | 194 |
| 5.1 Conclusion.....                          | 194 |
| 5.2 Further recommendation.....              | 195 |
| REFERENCES.....                              | 196 |
| APPENDICES.....                              | 220 |

## LIST OF FIGURES

|            |   | Pages |
|------------|---|-------|
| Figure 1.1 | The 10 Leading Causes of Death, 2011(WHO, 2013).  | 2     |
| Figure 1.2 | Effect of solid fuels smoke to human in various countries (WHO, 2014).  | 2     |
| Figure 1.3 | Child deaths due to selected causes in 2011(WHO, 2013).   | 2     |
| Figure 2.1 | Crystal structure and photograph of main polymorphs of TiO <sub>2</sub> (Augugliaro <i>et al.</i> , 2010).  | 14    |
| Figure 2.2 | A schematic diagram for the formation of charge carriers under UV light irradiation (Nakata and Fujishima, 2012).   | 20    |
| Figure 2.3 | A tentative mechanism of MB on C-N-doped TiO <sub>2</sub> . (MB, IB, FB and P represent methylene blue, intra-band-gap state, flat-band state and carbonaceous species, respectively) (Chen <i>et al.</i> , 2007a).   | 40    |
| Figure 2.4 | UV-Vis DRS spectra of on untreated Degussa P-25 TiO <sub>2</sub> films and Au/TiO <sub>2</sub> composite with Au surface loaded of (a) 0.4 μgcm <sup>-2</sup> , (b) 0.8 μgcm <sup>-2</sup> , (c) 1.6 μgcm <sup>-2</sup> and (d) 2 μgcm <sup>-2</sup> . (i) The left- hand side represent the wide range spectra while (ii) the right-hand side zooms in the irradiation region (350 nm) (Arabatzis <i>et al.</i> , 2003). | 42    |
| Figure 2.5 | A schematic mechanism of the photocatalytic reduction of water to H <sub>2</sub> (Yoong <i>et al.</i> , 2009).  | 47    |
| Figure 2.6 | TEM images of TiO <sub>2</sub> and Zr-TiO <sub>2</sub> (Swetha <i>et al.</i> , 2010).   | 49    |
| Figure 2.7 | Sources of indoor air pollution (Alpine Air Technologies, 2013).  | 60    |
| Figure 2.8 | Antibacterial effect on <i>E. coli</i> using disc diffusion method with: (a) commercial antibiotics. (b) Ag metal, Ag/TiO <sub>2</sub> particles, and AgNO <sub>3</sub> . (Keleher <i>et al.</i> , 2002).   | 65    |
| Figure 3.1 | A schematic diagram of TiO <sub>2</sub> synthesis used in this study.   | 71    |
| Figure 3.2 | A schematic diagram of cation-TiO <sub>2</sub> synthesis.   | 71    |
| Figure 3.3 | Annealing profile of TiO <sub>2</sub> .   | 73    |
| Figure 3.4 | Hydrothermal profile of TiO <sub>2</sub> synthesis.   | 73    |
| Figure 3.5 | The VOC monitoring apparatus at (a) A1- work station and (b) A9 – function room.  | 85    |

|             |  |     |
|-------------|--|-----|
| Figure 4.1  | Particle size and distribution of titania powder (prepared at pH 3) obtained from r ratio of (a) 25, (b) 50, (c) 75 and (d) 110.   | 95  |
| Figure 4.2  | TEM image of CR110-3.  | 98  |
| Figure 4.3  | XRD pattern of TiO <sub>2</sub> particles for pH 3 at water to Ti ratio of (a) 25, (b) 50, (c) 75 and (d) 110 annealed at 400 °C. (A: Anatase; B: Brookite).   | 100 |
| Figure 4.4  | FESEM image of titania nanoparticles for pH 3 at water to Ti ratio of (a) 25, (b) 50, (c) 75 and (d) 110 after annealing at 400 °C   | 101 |
| Figure 4.5  | MO degradation of TiO <sub>2</sub> nanoparticles prepared in various water to Ti ratio.  | 104 |
| Figure 4.6  | XRD patterns of TiO <sub>2</sub> annealed at 400 °C.   | 105 |
| Figure 4.7  | An illustration of rutile and anatase formation mechanism: (a) isolated octahedral in solution, (b) two octahedral join at vertex, (c) octahedral join along an edge. Cation-cation repulsion causes distortion, (d) third octahedron join the cluster at a corner, (e) rutile formation - linear array and (f) anatase formation- right angle array (Gopal <i>et al.</i> , 1997). | 107 |
| Figure 4.8  | FESEM images of pH variation on the titania nanoparticles: (a) pH 1(b) pH 3 and (c) pH 5 (d) pH 7 and (e) pH 9.  | 108 |
| Figure 4.9  | TEM images of TiO <sub>2</sub> annealed at 400 °C for 4 h using (a) CR110-3, (b) CR110-5, (c) CR110-7 and (d) CR110-9.   | 109 |
| Figure 4.10 | Particle size distribution of (a) CR110-1, (b) CR110-3, (c) CR110-5, (d) CR110-7 and (e) CR110-9.  | 110 |
| Figure 4.11 | FTIR spectra of TiO <sub>2</sub> annealed at 400 °C using (a) pH 1, (b) pH 3, (c) pH 5, (d) pH 7 and (e) pH 9.   | 112 |
| Figure 4.12 | MO degradation of TiO <sub>2</sub> annealed at 400 °C.   | 114 |
| Figure 4.13 | Kinetic rate constant of as-prepared samples photoactivity under UV light irradiation.   | 116 |
| Figure 4.14 | X-ray diffraction of TiO <sub>2</sub> prepared with water to Ti ratio of 110 at pH 3 with various annealing atmosphere condition: (a) air, (b) carbon and (c) nitrogen.  | 118 |
| Figure 4.15 | PL emission of TiO <sub>2</sub> prepared at pH 3 with different annealing atmosphere condition at 400 °C   | 120 |

|             |  |     |
|-------------|--|-----|
| Figure 4.16 | FTIR spectra of (a) CR110-3-C, (b) CR110-3-N and (c) CR110-3-Air.  | 121 |
| Figure 4.17 | MO degradation of the as-prepared samples under UV irradiation.  | 121 |
| Figure 4.18 | PCA of the as-prepared samples under UV light irradiation.   | 122 |
| Figure 4.19 | XRD patterns of TiO <sub>2</sub> prepared by hydrothermal treatment at 150 °C.   | 125 |
| Figure 4.20 | Particle size distribution of TiO <sub>2</sub> via hydrothermal treatment at 150 °C for 6 h as (a) H150-1, (b) H150-3, (c) H150-5, (d) H150-7 and (e) H150-9.                        | 126 |
| Figure 4.21 | TEM image of TiO <sub>2</sub> synthesized via sol gel method assisted hydrothermal treatment at 150 °C for 6 h with hydrolysis condition at pH (a) 1, (b) 3, (c) 5, (d) 7 and (e) 9. | 127 |
| Figure 4.22 | FTIR spectra of TiO <sub>2</sub> synthesized via sol gel method followed by hydrothermal at 150 °C um at (a) pH 1, (b) pH 3, (c) pH 5, (d) pH 7 and (e) pH 9.                        | 128 |
| Figure 4.23 | Comparison of the MO degradation under UV irradiation for 5 h duration.  | 129 |
| Figure 4.24 | EFTEM micrograph of TiO <sub>2</sub> nanosolution (a) P14-A; (b) P28-B.  | 131 |
| Figure 4.25 | Effect of peptization duration on the average particle size of TiO <sub>2</sub> .  | 132 |
| Figure 4.26 | TEM image of TiO <sub>2</sub> nanosolution peptized at 85 °C for 8 h.  | 132 |
| Figure 4.27 | XRD pattern of TiO <sub>2</sub> peptized at 85° for (a) 3 h and (b) 8 h.   | 134 |
| Figure 4.28 | A UV-Vis spectra of TiO <sub>2</sub> -P and the inset shows the band gap energy (E <sub>g</sub> ).   | 135 |
| Figure 4.29 | Photoluminescence spectra of TiO <sub>2</sub> .  | 136 |
| Figure 4.30 | PCA efficacy in term of TiO <sub>2</sub> catalyst loading.   | 137 |
| Figure 4.31 | MO degradation under UV light exposure using (a) TiO <sub>2</sub> -P and (b) blank.  | 137 |
| Figure 4.32 | The degradation of MO under xenon irradiation for 10 h:  | 138 |

|             |   |     |
|-------------|---|-----|
|             | (a) TiO <sub>2</sub> -P and (b) blank.  |     |
| Figure 4.33 | XRD diffractogram of (a) pure TiO <sub>2</sub> , (b) 3Fe-TiO <sub>2</sub> , (c) 5Fe-TiO <sub>2</sub> and (d) 8Fe-TiO <sub>2</sub> .   | 141 |
| Figure 4.34 | TEM images of (a) 3Fe-TiO <sub>2</sub> , (b) 5FeTiO <sub>2</sub> and (c) 8Fe-TiO <sub>2</sub> .   | 142 |
| Figure 4.35 | EDX spectrum of Fe-TiO <sub>2</sub> using (a) 3 mmol Fe, (b) 5 mmol Fe and (c) 8 mmol Fe.   | 143 |
| Figure 4.36 | MO degradation under UV light irradiation using Fe-TiO <sub>2</sub> synthesized via hydrothermal treatment at 150 °C for 6 h.   | 144 |
| Figure 4.37 | XRD diffractogram of TiO <sub>2</sub> and Fe-TiO <sub>2</sub> peptized at 85 °C for 8 h.  | 146 |
| Figure 4.38 | TEM image of Fe-TiO <sub>2</sub> peptized at 85 °C for 8 h. The inset shows the high magnification of the nanoparticles.  | 147 |
| Figure 4.39 | EDX spectrum of Fe-TiO <sub>2</sub> -P nanoparticles peptized at 85 °C for 8 h.   | 147 |
| Figure 4.40 | UV-Vis DRS spectrum of TiO <sub>2</sub> -P and Fe-TiO <sub>2</sub> -P. The inset shows the E <sub>g</sub> of both samples.  | 148 |
| Figure 4.41 | MO degradation of (a) Fe-TiO <sub>2</sub> -P and (b) TiO <sub>2</sub> -P nanosolution under UV light illumination   | 149 |
| Figure 4.42 | MO degradation of TiO <sub>2</sub> nanosolution under fluorescent light illumination for 10 h as (a) FeTiO <sub>2</sub> -P and (b) TiO <sub>2</sub> -P and (c) blank.                 | 150 |
| Figure 4.43 | XRD patterns of pure TiO <sub>2</sub> and Ag-TiO <sub>2</sub> as (a) pure TiO <sub>2</sub> , (b) 1 mmol Ag, (c) 2 mmol Ag, (d) 3 mmol Ag, (e) 4 mmol Ag and (f) 5 mmol Ag.            | 153 |
| Figure 4.44 | TEM images of (a) 1Ag-TiO <sub>2</sub> and (b) 5Ag-TiO <sub>2</sub> and (c) pure TiO <sub>2</sub> .   | 154 |
| Figure 4.45 | EDX spectrum of Ag-TiO <sub>2</sub> as (a) 1Ag-TiO <sub>2</sub> , (b) 2Ag-TiO <sub>2</sub> , (c) 3Ag-TiO <sub>2</sub> , (d) 4Ag-TiO <sub>2</sub> and (e) 5Ag-TiO <sub>2</sub> .       | 154 |
| Figure 4.46 | FT-IR spectra of (a) pure TiO <sub>2</sub> , (b) 1Ag-TiO <sub>2</sub> , (c) 2Ag-TiO <sub>2</sub> , (d) 3Ag-TiO <sub>2</sub> , (e) 4Ag-TiO <sub>2</sub> and (f) 5Ag-TiO <sub>2</sub> . | 156 |
| Figure 4.47 | Comparison of light absorption spectra of Ag-TiO <sub>2</sub> and pure TiO <sub>2</sub> .   | 157 |
| Figure 4.48 | The optical band gap energy of Ag-TiO <sub>2</sub> and pure TiO <sub>2</sub> prepared via peptization method.   | 157 |

|             |   |     |
|-------------|---|-----|
| Figure 4.49 | PCA of MO degradation under fluorescent light exposure using (a) blank, (b) pure TiO <sub>2</sub> and (c) 1Ag-TiO <sub>2</sub> .  | 158 |
| Figure 4.50 | Proposed mechanism of MO degradation by 1Ag-TiO <sub>2</sub> .  | 161 |
| Figure 4.51 | Cotton diffusion test for antibacterial strength using (a) Ag-TiO <sub>2</sub> , (b) TiO <sub>2</sub> and (c) control.  | 162 |
| Figure 4.52 | TEM image of <i>E. coli</i> bacteria: (a) untreated and (b) treated with Ag-TiO <sub>2</sub> .  | 163 |
| Figure 4.53 | Proposed mechanism of Ag-TiO <sub>2</sub> attack on <i>E.coli</i> .   | 164 |
| Figure 4.54 | Comparison of XRD diffractogram of (a) pure TiO <sub>2</sub> , (b) Zr-TiO <sub>2</sub> using method 1 and (c) Zr-TiO <sub>2</sub> using method 2.   | 166 |
| Figure 4.55 | XRD diffractogram of (a) pure TiO <sub>2</sub> , (b) 1Zr-TiO <sub>2</sub> , (c) 2Zr-TiO <sub>2</sub> , (d) 3Zr-TiO <sub>2</sub> and (e) 4Zr-TiO <sub>2</sub> .  | 168 |
| Figure 4.56 | EDX spectrum of (a) 1Zr-TiO <sub>2</sub> , (b) 2Zr-TiO <sub>2</sub> , (c) 3Zr-TiO <sub>2</sub> , and (d) 4Zr-TiO <sub>2</sub> .   | 169 |
| Figure 4.57 | UV-Vis DRS of Zr-TiO <sub>2</sub> nanosolution. The inset shows the E <sub>g</sub> of each Zr-TiO <sub>2</sub> .  | 170 |
| Figure 4.58 | MO degradation under fluorescent light irradiation using (a) 4Zr-TiO <sub>2</sub> , (b) 3Zr-TiO <sub>2</sub> , (c) 2Zr-TiO <sub>2</sub> , (d) 1Zr-TiO <sub>2</sub> , (e) TiO <sub>2</sub> and (f) blank.                    | 171 |
| Figure 4.59 | Comparison of PL spectra of (a) 4Zr-TiO <sub>2</sub> and (b) TiO <sub>2</sub> .   | 172 |
| Figure 4.60 | TEM image of 4Zr-TiO <sub>2</sub> peptized at 85 °C for 8 h.  | 172 |
| Figure 4.61 | Disc diffusion test for antibacterial strength using (a) 1Zr-TiO <sub>2</sub> , (b) 2Zr-TiO <sub>2</sub> , (c) 3Zr-TiO <sub>2</sub> and (d) 4Zr-TiO <sub>2</sub> .  | 173 |
| Figure 4.62 | XRD diffractogram of (a) TiO <sub>2</sub> , (b) 1Ag-TiO <sub>2</sub> , (c) 4Zr-TiO <sub>2</sub> , (d) Ag-1Zr-TiO <sub>2</sub> , (e) Ag-2Zr-TiO <sub>2</sub> , (f) Ag-3Zr-TiO <sub>2</sub> and (g) Ag-4Zr-TiO <sub>2</sub> . | 174 |
| Figure 4.63 | EDX image of (a) Ag-1Zr-TiO <sub>2</sub> , (b) Ag-2Zr-TiO <sub>2</sub> , (c) Ag-3Zr-TiO <sub>2</sub> , and (d) Ag-4Zr-TiO <sub>2</sub> .  | 175 |
| Figure 4.64 | The images of Ag-4Zr-TiO <sub>2</sub> via (a) TEM and (b) HRTEM.  | 176 |
| Figure 4.65 | (a) TEM image of Ag-Zr-TiO <sub>2</sub> nanoparticles prepared via peptization process at 85 °C and its mapping image of (b) Ti element, (c) O element, (d) Ag element and (e) Zr element.                                  | 177 |
| Figure 4.66 | UV-Vis DRS of as-prepared sample of Ag-Zr-TiO <sub>2</sub> and  | 178 |

|             |  |     |
|-------------|--|-----|
|             | pure TiO <sub>2</sub> . The inset shows the E <sub>g</sub> of Ag-Zr-TiO <sub>2</sub> .   |     |
| Figure 4.67 | PL spectra of (a) pure TiO <sub>2</sub> , (b) 4Zr-TiO <sub>2</sub> and (c) Ag- 4Zr-TiO <sub>2</sub> .  | 179 |
| Figure 4.68 | MO degradation under fluorescent irradiation using (a) Ag-4Zr-TiO <sub>2</sub> , (b) Ag-3Zr-TiO <sub>2</sub> , (c) Ag-2Zr-TiO <sub>2</sub> , (d) Ag-1Zr-TiO <sub>2</sub> , (e) TiO <sub>2</sub> and (f) blank. | 180 |
| Figure 4.69 | Disc diffusion test for antibacterial strength using (a) Ag-1Zr-TiO <sub>2</sub> , (b) Ag-2Zr-TiO <sub>2</sub> , (c) Ag-3Zr-TiO <sub>2</sub> and (d) Ag-4Zr-TiO <sub>2</sub> .                                 | 182 |
| Figure 4.70 | Inhibition zone against <i>E. coli</i> of: (a) Ag-1Zr-TiO <sub>2</sub> (b) Ag-2Zr-TiO <sub>2</sub> (c) Ag-3Zr-TiO <sub>2</sub> (d) Ag-4Zr-TiO <sub>2</sub> .   | 183 |
| Figure 4.71 | TEM micrograph of (a) 4Ag-Zr-TiO <sub>2</sub> and (b) commercial nanoYo as-received.   | 184 |
| Figure 4.72 | XRD diffractogram of (a) Ag-4Zr-TiO <sub>2</sub> and (b) commercial TiO <sub>2</sub> solution.   | 185 |
| Figure 4.73 | Light absorption of Ag-4Zr-TiO <sub>2</sub> and commercial TiO <sub>2</sub> solution.  | 186 |
| Figure 4.74 | Comparison of the photocatalytic activities of the samples under fluorescent irradiation for (a) blank, (b) nanoYo and (c) Ag-4Zr-TiO <sub>2</sub> .   | 187 |
| Figure 4.75 | Antibacterial strength using (a) Ag-Zr-TiO <sub>2</sub> , (b) nanoYo TiO <sub>2</sub> .  | 188 |
| Figure 4.76 | Comparison of VOC results of various location at REHDA building for 3 month duration.  | 193 |

## LIST OF TABLES

|            |   | Pages |
|------------|---|-------|
| Table 2.1  | Fundamental properties of TiO <sub>2</sub> (Fujishima <i>et al.</i> , 2008, Chen and Mao, 2007, Reyes-Coronado <i>et al.</i> , 2008). | 15    |
| Table 2.2  | An overview of TiO <sub>2</sub> research work conducted from 1970's to 2014.  | 18    |
| Table 2.3  | Several work conducted by researchers in effort to produce the TiO <sub>2</sub> nanoparticles via sol gel process.                    | 31    |
| Table 2.4  | An overview of work reported on cation doped TiO <sub>2</sub> from 1980's to 2014.  | 51    |
| Table 2.5  | An overview of Fe-TiO <sub>2</sub> , Ag-TiO <sub>2</sub> and Zr-TiO <sub>2</sub> research work conducted from 2000's to 2014.         | 53    |
| Table 2.6  | Summary of air pollution sources and their effects to health and environment.   | 61    |
| Table 2.7  | List of IAQ recommendation by Industry Code of Practice on Indoor Air Quality 2010 (DOSH, 2010).                                      | 62    |
| Table 2.8  | An overview of TiO <sub>2</sub> photocatalysis application.   | 66    |
| Table 2.9  | Comparison of water purification devices.   | 67    |
| Table 2.10 | Comparison of air purification devices.   | 68    |
| Table 3.1  | List of chemical and reagent specification.   | 70    |
| Table 3.2  | Parameters and variation of <i>r</i> value for TiO <sub>2</sub> synthesis.  | 76    |
| Table 3.3  | The pH variation and codename for TiO <sub>2</sub> nanoparticles.   | 77    |
| Table 3.4  | TiO <sub>2</sub> nanoparticles synthesized at pH 3 and annealed in various atmosphere condition.                                      | 78    |
| Table 3.5  | Parameters of Fe-TiO <sub>2</sub> synthesis using sol gel method aided hydrothermal treatment and peptization process.                | 79    |
| Table 3.6  | The amount of silver used in Ag-TiO <sub>2</sub> sepiated at 85 °C for 8 h.   | 79    |
| Table 3.7  | The amount of Zr(IV) propoxide used.  | 80    |
| Table 3.8  | Composition used for Ag-Zr-TiO <sub>2</sub> nanoparticles.  | 80    |
| Table 3.9  | The selected location for antibacterial performance measurement.  | 84    |

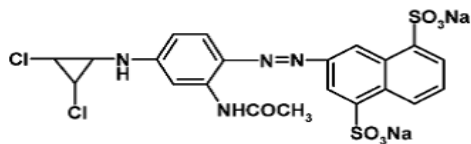
|            |  |     |
|------------|--|-----|
| Table 3.10 | The selected location of VOC measurement conducted at REHDA.   | 85  |
| Table 4.1  | Characteristic of TiO <sub>2</sub> synthesized by sol gel method assisted annealing at varying atmosphere condition for 4 h.                       | 100 |
| Table 4.2  | Crystallite size and specific surface area of sample prepared via sol gel method annealed at 400 °C.   | 107 |
| Table 4.3  | Kinetic analysis and PCA efficiency of TiO <sub>2</sub> annealed at 400 °C   | 115 |
| Table 4.4  | XRD results of TiO <sub>2</sub> annealed at 400 °C in varying atmosphere condition.  | 118 |
| Table 4.5  | Kinetic parameters and PCA efficacy of TiO <sub>2</sub> powder prepared in various annealed condition.   | 123 |
| Table 4.6  | Characterization results of TiO <sub>2</sub> nanocrystal prepared by hydrothermal treatment.   | 125 |
| Table 4.7  | Kinetic and PCA efficiency of TiO <sub>2</sub> prepared by hydrothermal treatment.   | 129 |
| Table 4.8  | Visual observation of the peptized TiO <sub>2</sub> stability.   | 130 |
| Table 4.9  | Summary of physicochemical properties of Fe-TiO <sub>2</sub> and pure-TiO <sub>2</sub> synthesized by hydrothermal treatment at 150 °C for 6 h.    | 141 |
| Table 4.10 | Kinetic parameters and photocatalyst performance of TiO <sub>2</sub> prepared by hydrothermal treatment at 150 °C.                                 | 144 |
| Table 4.11 | Characteristic of Fe-TiO <sub>2</sub> and pure-TiO <sub>2</sub> peptized at 85 °C for 8 h.   | 146 |
| Table 4.12 | Summary of Ag-TiO <sub>2</sub> characteristic synthesized via sol-gel method followed by peptization at 85 °C for 8 h.                             | 153 |
| Table 4.13 | Characteristic of Zr-TiO <sub>2</sub> peptized at 85°C for 8 h.  | 168 |
| Table 4.14 | Summary of physicochemical properties of Ag-Zr-TiO <sub>2</sub> synthesized by sol gel method followed by peptization process at 85 °C in for 8 h. | 175 |
| Table 4.15 | Zone of inhibition of Ag-Zr-TiO <sub>2</sub> .   | 183 |
| Table 4.16 | Swab test bacterial count.   | 189 |
| Table 4.17 | Comparison of Ag-Zr-TiO <sub>2</sub> and nanoYo.   | 190 |

|            |  |     |
|------------|--|-----|
| Table 4.18 | Antibacterial monitoring in selected location using swab test.   | 191 |
| Table 4.19 | Summary of TVOC count at REHDA building before and after applying TiO <sub>2</sub> solution for 3 month observation. | 192 |

## LIST OF ABBREVIATIONS

|                      |   |
|----------------------|---|
| REHDA                | Real Estate House Development Association           |
| NP                   | nanoparticles                                       |
| NS                   | nanosolution  |
| NT                   | nanotube  |
| IAQ                  | Indoor air quality                                  |
| IAP                  | Indoor air pollution                                |
| CB                   | Conduction band                                     |
| VB                   | Valence band  |
| PCA                  | Photocatalytic activity                             |
| ROS                  | Reactive oxygen species                             |
| MO                   | Methyl Orange                                       |
| MB                   | Methylene Blue                                      |
| Rh.B                 | Rhodamine B   |
| TTIP                 | Titanium(IV) isopropoxide                           |
| IP                   | 2-propanol/ Isopropanol                             |
| DI                   | Deionized water                                     |
| ESR                  | Electron spin resonance                             |
| CO <sub>2</sub> -TPD | CO <sub>2</sub> - temperature programmed desorption |
| VOC                  | Volatile Organic Compound                           |
| TVOC                 | Total Volatile Organic Compound                     |
| BET                  | Brunauer-Emmet-Taylor                               |
| FESEM                | Field Emission Scanning Electron Microscopy         |
| XRD                  | X-ray Diffraction Spectroscopy                      |
| TEM                  | Transmission Electron Microscopy                    |

|        |  |
|--------|--|
| HRTEM  | High Resolution Transmission Electron Microscopy                           |
| PL     | Photoluminescence  |
| UV-Vis | Ultra Violet-Visible   |
| XRG    | Organic dye with yellow colour. The molecular structure of XRG is as below |



## LIST OF SYMBOLS

|           |                           |
|-----------|---------------------------|
| %         | Percentage                |
| <         | Less than                 |
| >         | More than                 |
| °         | Degree                    |
| °C        | Degree Celsius            |
| °C/min    | Degree Celsius per minute |
| T         | Temperature               |
| L         | Litre                     |
| m         | Meter                     |
| cm        | Centimetre                |
| mL        | Millilitre                |
| mm        | Millimetre                |
| nm        | Nanometer                 |
| wt %      | Weight percent            |
| at.%      | Atomic percent            |
| mmol      | millimoles                |
| g         | Gram                      |
| $\lambda$ | Wave length               |
| h         | Hour                      |
| min       | Minute                    |
| s         | Second                    |

## LIST OF PUBLICATIONS & AWARDS

### Publications

1. IBRAHIM, S. A. & SREEKANTAN, S (2011). Effect of pH on TiO<sub>2</sub> Nanoparticles via Sol-Gel Method. *Advanced Materials Research*, 173, 184-189.
2. IBRAHIM, S. A., RIDHUAN, N. S. & SREEKANTAN, S. of methyl orange using TiO<sub>2</sub> as photocatalyst. AIP Conference Proceedings, 2011. 123-127.
3. IBRAHIM, S. A. & SREEKANTAN, S.(2010). Effect of annealing atmosphere towards TiO<sub>2</sub> nanoparticles on their photocatalytic performance in aqueous phase. *Proceeding of International Conference on Enabling Science and Nanotechnology (ESciNano 2010)*, 1- 3<sup>rd</sup> December 2010, Kuala Lumpur, Malaysia
4. IBRAHIM, S. A. & SREEKANTAN, S. (2014). Fe-TiO<sub>2</sub> Nanoparticles by Hydrothermal Treatment with PCA Enhancement. *Advanced Materials Research*. 1024, 39-43.
5. IBRAHIM, S. A. & SREEKANTAN, S. (2015). Effect of Fe Incorporation on the Photocatalytic Activity of TiO<sub>2</sub> by Sol-Gel Method. *Advanced Materials Research*. 1087, 218-222.

### Award

1. The Silver Medal, Korea International Women's Invention Exposition (KIWI) 2012, Seoul, Korea, 3-6 May 2012 for project entitles: SMARTCOAT: Remedy for VOC, Bacteria and Fungi growing world.
2. The Gold Medal, The British Invention Show (BIS) 2012, London, UK, 24-27 Oct 2012, for project entitle: SMARTCOAT-for natural earth category
3. The Gold Medal, The British Invention Show (BIS) 2012, London, UK, 24-27 Oct 2012, for project entitle: SMARTCOAT-for consumer category
4. The Gold Medal, National Research & Innovation Competition 2012, 17 - 19thJuly 2012, for project entitle: NANOCOAT: An Inspired Molecular Solutions for ultimate protection against indoor air pollutants
5. The Gold Medal, Malaysia Technology Expo 2013, 21-23<sup>rd</sup> Feb 2013, for project entitle: SMARTCOAT: Remedy for VOC, Bacteria and Fungi growing world.

# **PEMBANGUNAN TITANIUM DIOKSIDA NANOZARAH/LARUTAN-NANO UNTUK AKTIVITI FOTOPEMANGKIN**

## **ABSTRAK**

Bahan pencemar biologi dan kimia oleh aktiviti buatan manusia telah menjadi isu global yang serius. Pendedahan kepada bahan pencemar ini yang melebihi had boleh menyebabkan masalah alam sekitar dan kesihatan yang serius. Oleh itu, pembangunan penyelesaian berkesan yang boleh digunakan oleh manusia sejagat adalah penting. Salah satu cara berkesan untuk mengatasi masalah ini ialah dengan menggunakan titanium dioksida ( $\text{TiO}_2$ ).  $\text{TiO}_2$  adalah fotopemangkin yang diketahui umum dan digunakan dengan meluas bagi tujuan pembersihan alam sekitar disebabkan oleh keupayaannya untuk menguraikan bahan cemar organik dan membunuh bakteria. Walaupun  $\text{TiO}_2$  terbukti mempunyai kelebihan untuk menyelesaikan masalah ini, akan tetapi kebergunaannya terhad hanya kepada penyinaran cahaya UV. Oleh itu, tujuan kajian ini adalah untuk menyiasat potensi  $\text{TiO}_2$  yang boleh diaktifkan dalam cahaya nampak dengan gabungan ion logam (Fe, Ag, Zr dan Ag-Zr). Dalam kajian ini, kaedah sol-gel digunakan untuk mensintesis  $\text{TiO}_2$  yang digabungkan dengan ion logam. Analisis XRD menunjukkan semua sampel mempunyai anatas-brukit  $\text{TiO}_2$  dwifasa dengan saiz 3 nm hingga 5 nm. Penggabungan ion-ion logam didapati tidak mengubah morfologi  $\text{TiO}_2$  tetapi mempunyai kesan terhadap ciri-ciri kehabluran dan optik. Kehabluran anatas bagi  $\text{TiO}_2$  dwifasa didapati berkurangan dan pembentukan brukit diutamakan. Analisis PL menunjukkan penggabungan dengan ion-ion logam menghalang penggabungan semula pasangan elektron-lubang manakala tenaga sela jalur bagi  $\text{TiO}_2$  (3.2 eV) berkurangan apabila digabungkan dengan Fe (2.46 eV) dan Ag (2.86 eV). Antara

penggabungan ini, Ag-Zr yang digabungkan dengan TiO<sub>2</sub> menunjukkan prestasi tertinggi bagi degradasi metil jingga (93%) di bawah penyinaran cahaya pendarfluor selama 10 jam. Ini diikuti oleh Zr-TiO<sub>2</sub> (82%), Fe-TiO<sub>2</sub> (75%) dan Ag-TiO<sub>2</sub> (43%). Sementara itu, prestasi antibakteria tertinggi ditunjukkan oleh Ag-TiO<sub>2</sub>. Imej TEM menunjukkan bakteria *E.coli* dibunuh dalam jangka masa 12 jam selepas dirawat menggunakan Ag-TiO<sub>2</sub>. Keputusan yang diperolehi daripada kajian kerja lapangan membuktikan bahawa penggabungan dengan Ag-Zr mempunyai prestasi yang cemerlang bagi penyingkiran sebatian organik mudah meruap (VOC) dan ujian antibakteria. Kandungan VOC setelah dirawat oleh Ag-Zr-TiO<sub>2</sub> memenuhi Tataamalan Industri Kualiti Udara Dalaman 2010, iaitu lebih rendah daripada 3 ppm. Di samping itu, peratusan mikrob juga didapati berkurangan sekitar 45% dalam tempoh pemerhatian selama 5 hari.

**DEVELOPMENT OF TITANIUM DIOXIDE  
NANOPARTICLES/NANOSOLUTION FOR PHOTOCATALYTIC  
ACTIVITY**

**ABSTRACT**

Biological and chemical contaminants by man-made activities have been serious global issue. Exposure of these contaminants beyond the limits may result in serious environmental and health problem. Therefore, it is important to develop an effective solution that can be easily utilized by mankind. One of the effective ways to overcome this problem is by using titanium dioxide ( $\text{TiO}_2$ ).  $\text{TiO}_2$  is a well-known photocatalyst that widely used for environmental clean-up due to its ability to decompose organic pollutant and kill bacteria. Although it is proven  $\text{TiO}_2$  has an advantage to solve this concern, its usefulness unfortunately is limited only under UV light irradiation. Therefore, the aim of this work was to investigate the potential of  $\text{TiO}_2$  that can be activated under visible light by the incorporation of metal ions (Fe, Ag, Zr and Ag-Zr). In this study, sol-gel method was employed for the synthesis of metal ions incorporated  $\text{TiO}_2$ . XRD analysis revealed that all samples content biphasic anatase-brookite  $\text{TiO}_2$  of size 3 nm to 5 nm. It was found that the incorporation of these metal ions did not change the morphology of  $\text{TiO}_2$  but the crystallinity and optical properties were affected. The crystallinity of anatase in the biphasic  $\text{TiO}_2$  was found to be decreased and favored brookite formation. PL analysis showed metal ions incorporation suppressed the recombination of electron-hole pairs while the band gap energy of  $\text{TiO}_2$  (3.2 eV) was decreased by the incorporation of Fe (2.46 eV) and Ag (2.86 eV). Among this incorporation, Ag-Zr incorporated  $\text{TiO}_2$  showed highest performance for methyl orange degradation (93%) under fluorescent

light irradiation for 10 h. This follows by Zr-TiO<sub>2</sub> (82%), Fe-TiO<sub>2</sub> (75%) and Ag-TiO<sub>2</sub> (43%). Meanwhile, the highest antibacterial performance was exhibited by Ag-TiO<sub>2</sub>. TEM images showed that *E.coli* bacterium was killed within 12 h after treated with Ag-TiO<sub>2</sub>. The results obtained from the fieldwork study established that Ag-Zr incorporation have excellent performances for VOC removal and antibacterial test. The VOC content after treated with Ag-Zr-TiO<sub>2</sub> fulfilled the Industry Code of Practice on Indoor Air Quality 2010 which is lower than 3 ppm. In addition, the percentage of microbes also found to be decrease around 45 % within 5 days of monitoring.

# CHAPTER1

## INTRODUCTION

### 1.1 Introduction

According to World Health Organization (WHO), environment-related problem is one of the top ten causes of death worldwide, contributing towards 23% of global diseases. Among the ten leading causes of death, half of the causes are related to indoor air pollutants. It is estimated to kill 4.3 million people yearly (Figure 1.1). Serious health issues such as allergies, headaches, and respiratory problems, intestinal and cardiovascular diseases are resulted from poor indoor air quality (IAQ) (Carneiro *et al.*, 2007, Liu *et al.*, 2011, Brugha and Grigg, 2014). It is reported that indoor air pollution (IAP) is more harmful five times higher than outdoor air. Most people spend 80-90% time doing indoor activities, thus good indoor environment is essential towards human fitness to work efficiency. In general, temperature, air movement, humidity, ventilation, air exchange rate and various pollutants such as biological, gaseous and particulate affects IAQ (Lin *et al.*, 2014, Liu *et al.*, 2010).

Figure 1.2 best illustrates the IAP deaths at various regions worldwide. Obviously, Africa is the highest IAP affected continent followed by Asia countries including South East Asia. Premature death for children below 5 years was approximately 3.2 million in Africa, 2 million deaths in South East Asia and 1.7 million in the rest of world (Figure 1.3). Majority of them are affected by pneumonia and chronic obstructive pulmonary disease (COPD).

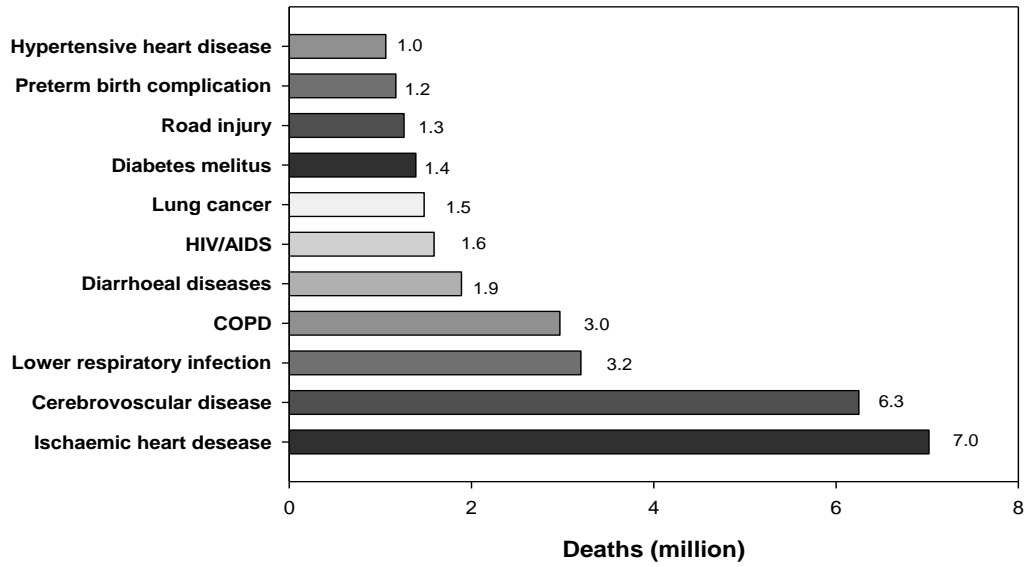


Figure 1.1. The 10 Leading Causes of Death, 2011(WHO, 2013).

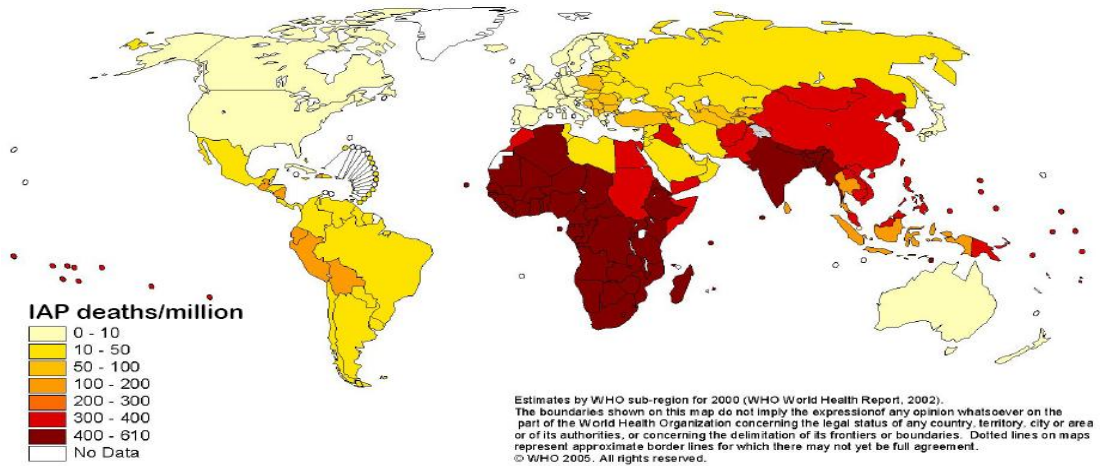


Figure 1.2. Effect of solid fuels smoke to human in various countries (WHO, 2014).

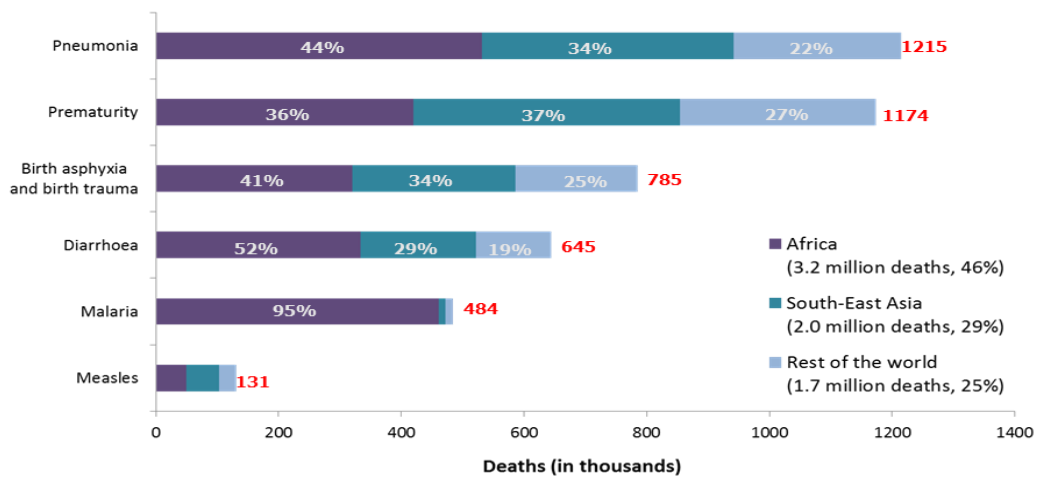


Figure 1.3. Child deaths due to selected causes in 2011(WHO, 2013).

Other than air, water pollution also is another issue that needs attention. Poor water quality affects the living organisms and ecosystem. Water can be contaminated either through biological or chemical compound originated from industrial effluents, residential sewage and human activities. Poor water quality can bring major outbreak diseases including diarrheal diseases, malaria and Legionnaires' disease (Törnqvist *et al.*, 2011). For example, in Africa malaria disease contributes the highest death for children with 645,000 counts and diarrhea about 484,000 counts (Figure 1.3).

In order to solve this issue, an extensive works on various technology are carried out and among those technologies, advanced oxidation process (AOP) is one of the most promising alternative technologies to perform environmental clean-up process (Anpo and Kamat, 2010). AOP development includes the use of Fenton process, ozonation and/or photocatalyst for of pollutants and pathogens removal (Catalkaya and Kargi, 2007, Arslan-Alaton, 2007, Hochmannova and Vytrasova, 2010). In this research work, photocatalyst reaction utilizing nano-TiO<sub>2</sub> is selected due to its chemical stability, good mechanical properties, non-toxic and has high efficacy in degrading organic pollutant (Obee and Brown, 1995, Hänel *et al.*, 2011). This state of technology utilizes UV light to generate electron and holes. The holes oxidize the water and the electrons reduce the oxygen in the atmosphere to form strong oxidation reactant: hydroxyl radical (OH<sup>•</sup>) and superoxide anion (O<sub>2</sub><sup>•-</sup>). These reactants decompose toxic pollution through oxidation to form harmless substances such as carbon dioxide (CO<sub>2</sub>) and water.

## 1.2 Problem Statement

TiO<sub>2</sub> photocatalyst is much appreciated in recent years for energy harvesting and environmental remediation due to high catalytic activity, good chemical and mechanical stability, cost effective and inert to human beings and environment (Fujishima *et al.*, 2000, Chen and Mao, 2007). However, this material requires UV irradiation to be activated. This is due to the intrinsic band gap of TiO<sub>2</sub> (anatase = 3.2 eV; rutile = 3.0 eV), which requires energy source with wavelength  $\leq$  390 nm. UV rays consists three types of ray such as UVA (390-315 nm); UVB (315-280 nm) and UVC (280-100 nm). Among these three, UVA and UVB rays can cause genetic damage and skin cancer, thus cause adverse health effect to mankind (Braun, 2008). Meanwhile, a ray of UVC could not reach earth as it is completely absorbed by ozone layer. This restriction hinders the photocatalytic process to be economically sound. If UV light is the source of radiation, the photocatalytic process must be conduct in a closed environment, which limits the usage for indoor application.

In response with aforementioned deficiencies, several approaches have been conducted to extend the absorption to the visible light wavelength. These includes the investigation on the effect of various synthesis parameters such as preparation techniques (Byun *et al.*, 2000, Yoshida *et al.*, 2005, Ismail *et al.*, 2013), temperatures (Tang *et al.*, 2003, Górska *et al.*, 2008), pH values (Sun and Gao, 2002, Fumin *et al.*, 2007), precursor type, heat treatment and chemical composition (Doeuff *et al.*, 1987, Karvinen, 2003, Ananpattarachai *et al.*, 2009). Among those, heat treatment process has an essential role in determining the crystal structure of TiO<sub>2</sub> nanoparticles. Crystallization of amorphous TiO<sub>2</sub> to anatase phase occurs at the range of 250-400 °C while transformation from anatase to rutile occurs at 500 °C to 1000 °C (Yu *et*

*al.*, 2003, Prasad *et al.*, 2010, Faycal Atitar *et al.*, 2015). The ability to control crystal structure of TiO<sub>2</sub> could offer advantages for the enhancement of photocatalytic activity (Mahshid *et al.*, 2009). However, heat treatment such as calcination accelerates particle growth and induce agglomerates, thus led to photocatalytic activity (PCA) reduction (He *et al.*, 2014). Therefore, in this work an alternative method such as hydrothermal and peptization is used to produce smaller particle size with high crystallinity. Hydrothermal is selected because this treatment involves a reaction occurring at temperature 140 °C to 300 °C in aqueous in a closed system with high pressure (Wahi, 2005, Hidalgo *et al.*, 2007a, Phan *et al.*, 2009). This treatment provides longer condensation process in the presence of heat and pressure which induces the formation of smaller particle size. On the other hand, peptization is conducted at temperature below 100 °C to induce the formation of stable dispersion of colloidal particles. Bischoff and Anderson (1995) and Mahshid *et al.* (2007) that the presence of peptizing agent such as acid process promotes the breakup of bigger aggregates into smaller one due to electrostatic repulsion of the charged particle.

Obviously, retention of small particle size with good crystallinity is the focus of this work to perform high PCA efficiency. The reduction of size would cause electronic modification, resulting either in the enhancement or a suppression of the electrons and holes activities due to absorbed photon energies (Anpo *et al.*, 1987). Zhang *et al.* (1998) reported that particle size plays a crucial factor for dynamic electron- holes pairs recombination. Smaller particle size introduced high number of active surface sites and the surface charge carriers transfer rate in photocatalysis (Jang *et al.*, 2001a, Moiseev *et al.*, 2013). Furthermore, several literatures reported

that nanosized semiconductor with particle size less than 10 nm show significant enhancement on photocatalytic reactivity due to the quantum size (Q-sized effect). Kormann *et al.* (1988) reported that a number of semiconductor showed blue-shift absorption band edge as the size is reduced in consequence of exciton confinement. Anpo and co-workers suggested that the Q-sized effect modified the energy level in the localized photoexcited state of TiO<sub>2</sub> photocatalyst. In other words, the particle reduction increased the ratio of the surface to the bulk, resulting to the photogenerated electron-hole pairs can easily and quickly diffused to the surface of the catalyst. This activity forms the active sites at which the PCA (redox) reactions are induced (Anpo *et al.*, 1988, Anpo and Takeuchi, 2003). Choi *et al.* (1994) partially supported this idea as their study confirmed that undoped Q-sized TiO<sub>2</sub> showed blue-shift while doping it with metal ions increased the absorption edge to visible region (red-shifted). Therefore in this work, sol-gel assisted with peptization or hydrothermal is used to obtain an optimal particle size and stable TiO<sub>2</sub> nanosolution for high PCA performance.

Other than that, different approach such as sacrificial reagents addition (hole scavengers), photosensitization by an appropriate dye (Castro *et al.*, 2012), ion doping with foreign element ( noble or transition metals) and anionic species such as N,C and F are reported in literatures for PCA enhancement (Dvoranová *et al.*, 2002, Kobayakawa *et al.*, 2005, Wohlgemuth *et al.*, 2012). The alteration of electronic structure of TiO<sub>2</sub> by incorporating TiO<sub>2</sub> lattice with foreign element was found to enhance the PCA performance. Recent study by Pugazhenthiran *et al.* (2014) also confirmed that Q-sized TiO<sub>2</sub> doped with metal extended the absorption wavelength

to 560 nm and enhanced PCA under visible region. Therefore, tuning the band gap energy to visible range is essential.

In this work, cation incorporation (Fe, Ag, Zr and Ag-Zr) were used in order to improve the photocatalytic activity under visible light irradiation. It was postulated that the incorporation of Fe and Zr could narrow the band gap energy and widen the light absorption range into visible region. Meanwhile Ag incorporation could enhance the quantum efficiency by suppressing the recombination of photogenerated electrons and holes as the ions acts as electron traps. To note, the term cation incorporation was used in order to describe the presence of impurities in TiO<sub>2</sub> system instead of cation doping. The term cation incorporation signifies the presence of impurities either by substitutional and/or interstitial in TiO<sub>2</sub> lattice or deposited on the TiO<sub>2</sub> surface itself. On the other hand, cation doping signifies the presence of cation in the lattice by substituting Ti<sup>4+</sup> due to the similarity of their ionic radius.

Another aspect which of a great interest that is the antibacterial nature of TiO<sub>2</sub>. Study on the antibacterial properties was conducted by Ubonchonlakate *et al.* (2012) using Ag doped TiO<sub>2</sub> on *P.aeruginosa* as bacteria agent. The results showed that Ag doped TiO<sub>2</sub> have antibacterial effect as 100% of *P.aeruginosa* is disinfected in 10 minutes under UV light irradiation. In another study, Wang *et al.* (2013) synthesized TiO<sub>2</sub> that successfully degraded methylene blue (MB) and eliminated bacteria such as *E.coli* and *P.aeruginosa*. However, not much work has been investigated on the performance of this material under visible light exposure. It is also reported in literatures that doping TiO<sub>2</sub> with other elements (such as Cu, Pt, N and F) could enhance the absorption of photon energy under visible response (Chen

*et al.*, 2013, Dashora *et al.*, 2014, Fan *et al.*, 2008, Zhou *et al.*, 2008). Therefore, the used of cation incorporation TiO<sub>2</sub> sample for PCA that includes the antibacterial effect needs to be elucidated. The best formulation to have PCA is proposed and the efficacy is measured under lab scale and site test in several location (such as: Real Estate House Development Association or known as REHDA, Petaling Jaya; CIMB Commerce Square Level 6, Bukit Damansara; Chrisdale and Little Mandarin House kindergartens, Bangsar). These places were selected due to high human activities that may increase the VOC pollutants in air and bacterial growth.

### **1.3 Objectives**

The objectives of this research are describes as follows:

- 1) To synthesize nanosize pure-TiO<sub>2</sub> and cation incorporated TiO<sub>2</sub> (Ag, Fe, Ag-Zr) using sol gel method.
- 2) To investigate the properties of TiO<sub>2</sub> and cation incorporated TiO<sub>2</sub> under different post-heat treatments (annealing/hydrothermal/peptization).
- 3) To determine the photocatalytic activity of pure-TiO<sub>2</sub> and cation-TiO<sub>2</sub> using methyl orange degradation and bacteria elimination (*E.coli*) under visible light irradiation.
- 4) To measure the effectiveness of cation-TiO<sub>2</sub> for VOC removal and antimicrobial property at field work (REHDA, Petaling Jaya; CIMB Commerce Square, Bukit Damansara; kindergartens: Chrisdale and Little Mandarin House 1 & 2, Bangsar).

#### **1.4 Scope of work**

This project is conducted to produce fine-TiO<sub>2</sub> nanoparticles with good crystallinity that capable for organic removal with antibacterial property. In order to achieve the desired characteristic, sol gel method subsequently aided by heat treatment (annealing, hydrothermal or peptization) was selected. The purposes for using three different methods are to compare the characteristic and properties of those materials with pure TiO<sub>2</sub>. At the end of the process, the best method is selected to produce stable TiO<sub>2</sub> in nanosolution form that has the desired properties for organic removal and antibacterial effect. The parameters investigated for this study include water to Ti ratio and pH of hydrolysis medium. This is followed by incorporation of cation (Fe, Ag, Zr and Ag-Zr) into TiO<sub>2</sub> to enhance the visible response. TiO<sub>2</sub> that can perform PCA and antibacterial under visible light was expected as an output of this work. The best result obtained from optimised formulation TiO<sub>2</sub> is then selected for case studies in selected location. The volatile organic compound (VOC) removal and antibacterial property are monitored and reported in here.

#### **1.5 Thesis overview**

This thesis consists five chapters. Chapter 1 describes a brief introduction, problem statement, objective, expected outcome and scope of research work. In Chapter 2, a comprehensive review on the principle of photocatalyst, TiO<sub>2</sub> fabrication, modification of TiO<sub>2</sub> by incorporating noble metal, metal ion and anion doping in TiO<sub>2</sub> system for PCA enhancement and the functionality including water and air treatment and antibacterial are elaborated. The details of experimental work conducted in this study are discussed Chapter 3. This includes the experimental

design, the preparation of pure TiO<sub>2</sub> and cation-TiO<sub>2</sub> nanoparticles/nanosolution synthesis, functionality studies and case study procedures for VOC and antibacterial monitoring. In addition, the characterization techniques are also described in details including characterization equipment, their operation principle and sample preparation.

Chapter 4 presents the experimental results and comprehensive discussion on the formation of TiO<sub>2</sub> nanoparticles/nanosolution via sol gel method subsequently followed by heat treatment process (annealing/hydrothermal/peptization) and their application as photocatalyst and antibacterial material. The content was organized into three parts including (1) the details investigation on pure TiO<sub>2</sub> synthesis as a function of the effect of water to Ti molar ratio and pH via annealing and hydrothermal treatment. The optimum condition was established and replicated for next modification in term of size reduction using peptization process, (2) the incorporation of cation into TiO<sub>2</sub> system for PCA enhancement under visible light response by introducing Fe, Ag and Zr in the synthesis process, including the functionality study consist of MO degradation and antibacterial effect and (3) the PCA performance of the optimized TiO<sub>2</sub> at selected location (REHDA building, CIMB Commerce Square and kindergartens).

## CHAPTER 2

### LITERATURE REVIEW

#### 2.1 Introduction

Concern on environmental problems related to toxic air pollutants and hazardous wastes and contaminated groundwater and soils are global issue (Wolterbeek, 2002, Percy and Ferretti, 2004, Petrić *et al.*, 2011). The environment was contaminated due to the human mistakes, being ignorance since the past and present behavior. These are due to our conducts as we are totally dependent with things that contributed to global pollution by using hydrocarbon fuels for energy, industrial processes which produced hazardous wastes like heavy metal, dye and others. To improve the air quality, extensive research work by various researchers comes out with plenty technologies as antidote. For examples; the usage of tree as bio-indicator for heavy metal (Sawidis *et al.*, 2011), the usage of bacterial cell for degradation of textile wastewater (Pearce *et al.*, 2003), filtration (Hedberg *et al.*, 2011) and oxidation process (Deiber *et al.*, 1997, Magureanu *et al.*, 2005, Arslan-Alaton, 2007). However, not all methods mentioned above can be used in various environments or easily adopted in existing technology. Some method is very expensive, applicable only in selective environment or condition, high maintenance and difficult to handle. Therefore, scientist continuously looking and developing new ways to address this issue. Based on literatures review, the developments of new catalytic and photocatalytic processes provide great help to address this problem. These material based-catalyst has great potential in controlling water contaminant or air pollutants (Lloyd, 2006, Vandenbroucke *et al.*, 2011). It is believed that the material based-catalyst have several advantages over conventional oxidation process, such as: (1) complete mineralization of the pollutants; (2) use near UV or solar light;

(3) can be operated in room temperature, (4) safe, clean and efficient and (5) easily co-exist harmoniously with the environment (Herrmann, 1999, Anpo and Takeuchi, 2003, Catalkaya and Kargi, 2007, Zhai *et al.*, 2010).

One of the promising catalyst-based materials is TiO<sub>2</sub> or also known as titania. TiO<sub>2</sub> is a semiconductor photocatalyst and has been proven suitable for various environmental applications due to its stability, strong oxidizing powers, non-toxicity materials, ready availability and low cost (Linsebigler *et al.*, 1995, Fujishima *et al.*, 2000, Fujishima *et al.*, 2008, Hashimoto *et al.*, 2005). As photocatalyst, TiO<sub>2</sub> required the presence of light to decompose organic materials. The most important forms of TiO<sub>2</sub> are anatase, rutile and brookite. Among these crystals, anatase has been proven as an excellent photocatalyst when compared to rutile and brookite. It is reported that high crystallinity of anatase offers fewer defects acting as recombination sites between photogenerated electrons and holes. In another study Luttrell *et al.* (2014) described that the lifetime of charge carriers is high in anatase when compared to rutile, indicating high PCA. On the other hand, brookite is seldom studied because of the complicated synthesis procedure (Di Paola *et al.*, 2013). Unfortunately, the major drawback of TiO<sub>2</sub> is that the photoexcitation process activated only under UV irradiation which 5% of the solar light that reached on the earth surface. In order to improve the photocatalytic efficiency under visible light region, considerable effort have been made by many scientist (Stathatos *et al.*, 2001, Livraghi *et al.*, 2005, Górska *et al.*, 2008, Wang *et al.*, 2008). Consequently, tuning TiO<sub>2</sub> with metal and/or non-metal materials may alter the wavelength absorption of the photocatalyst. The photoactivity of doped photocatalyst may also be improved or declined depending on several factors such as the concentration or amount (Choi *et*

*al.*, 1994, Fan *et al.*, 2008) and the dopant ion nature (Safronova and Yaroslavtsev, 2013). The properties of metal doped TiO<sub>2</sub> is also depended on the dopant ion nature. Dopant ion nature includes the valence state, ionic radius, and chemical property. For example, by doping TiO<sub>2</sub> with metal ion that has lower valence state than Ti<sup>4+</sup> would produce oxygen vacancies to compensate the charge balance. The increased number of oxygen vacancies could enhance the PCA. Another group believed that by manipulating the preparation method and the thermal treatment produced superior photocatalyst with high surface area and crystallinity which correlated to photocatalytic performance (Zhang *et al.*, 2000, Kominami *et al.*, 2003, Maeda and Watanabe, 2007). In the subsequent section, the historical overview, basic principle of photocatalyst, reviews on pure TiO<sub>2</sub> and tuned-TiO<sub>2</sub> synthesis done by various researchers and the functionality will be reviewed in details.

## 2.2 TiO<sub>2</sub> nanoparticles

Titanium dioxide (TiO<sub>2</sub>) or titania exists in a number of crystalline forms and the most important phases are anatase, rutile and brookite. Each of them has different crystal structure but is expressed in the same chemical formula of TiO<sub>2</sub>. For better understanding, Figure 2.1 illustrates the crystal structure and images of each polymorph. Naturally, TiO<sub>2</sub> is extracted from ilmenite or leucocene ores and also can readily be mined in rutile beach sand. Normally TiO<sub>2</sub> occurs in white solid powder and usually applied as white pigment for paints, cosmetic, medicine and food industries.

TiO<sub>2</sub> have a bonding of O=Ti=O with a molar mass of 79.87 g/mole. The melting point of TiO<sub>2</sub> is at 1850 °C while the boiling temperature is at 2972 °C. In

addition, the density of  $\text{TiO}_2$  is approximately at  $4.23 \text{ g/cm}^3$ . It is also known as n-type semiconductor with band gap energy ( $E_g$ ) of 3.0 eV for rutile and 3.2 eV for anatase. Due to these large band gaps, the photocatalytic property of  $\text{TiO}_2$  is applicable under the UV illumination. The stability of various  $\text{TiO}_2$  phases depends on the size. It is reported that rutile is the most stable when the particle size is above 35 nm. Meanwhile, anatase and brookite is stable when the particle size is in the range of  $< 11 \text{ nm}$  and  $11\text{-}35 \text{ nm}$ , respectively (Fujishima *et al.*, 2008). A study by Ovenstone and Yanagisawa (1999) revealed that anatase structure formed at temperature  $< 450 \text{ }^\circ\text{C}$  while rutile appeared at much higher temperature at  $600 \text{ }^\circ\text{C}$  and above.

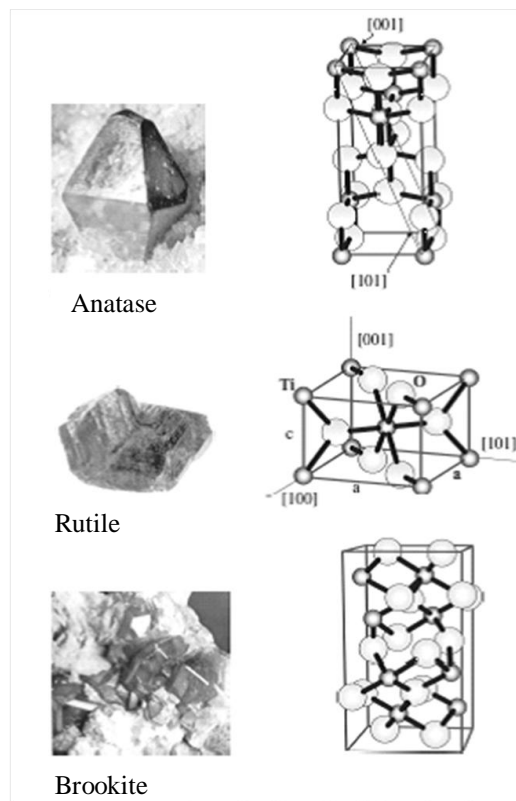


Figure 2.1. Crystal structure and photograph of main polymorphs of  $\text{TiO}_2$  (Augugliaro *et al.*, 2010).

The physical and mechanical properties of sintered titanium dioxide are tabulated in Table 2.1. Although anatase has higher band gap energy, the PCA of anatase is obviously superior when compared to rutile and brookite. Anatase is more favorable for PCA due to its high adsorptive affinity towards organics species and lower charge recombination rate than rutile (Linsebigler *et al.*, 1995, Sclafani and Herrmann, 1996). Moreover, the lifetime of photogenerated electrons and holes in anatase is longer than in rutile, hence enhancing the chance of photoexcited electrons and holes in anatase to participate in surface chemical reaction (Xu *et al.*, 2011). Although brookite has smaller band gap energy than anatase, it is difficult to synthesize brookite. Usually brookite is present together with anatase or rutile, forming a mixed phase in TiO<sub>2</sub>.

Table 2.1. Fundamental properties of TiO<sub>2</sub> (Fujishima *et al.*, 2008, Chen and Mao, 2007, Reyes-Coronado *et al.*, 2008).

|                              | <b>Anatase</b> | <b>Brookite</b> | <b>Rutile</b> |
|------------------------------|----------------|-----------------|---------------|
| Band gap                     | 3.2 eV         | 3.13 eV         | 3.0 eV        |
| Excitation wavelength (nm)   | 390 nm         | 380 nm          | 405 nm        |
| Refractive index             | 2.49           | 2.7             | 2.903         |
| Density (gcm <sup>-3</sup> ) | 3.84           | 4.133           | 4.26          |
| Crystal Structure            | tetragonal     | orthorhombic    | tetragonal    |

### 2.3 Historical overview

Originally, TiO<sub>2</sub> has been used mostly as white pigment. Rutile has been chosen for this purpose since it can be obtain in natural abundance. However, with the introduction of semiconductor and the emerging of nanotechnology, the application of TiO<sub>2</sub> has been boost up and those applications are linking together with anatase phase. In 1972, Fujishima made a breakthrough discovery for water

photolysis by electrochemical using  $\text{TiO}_2$ . It was discovered that rutile as electrodes could split water and produced hydrogen. Since then, countless studies towards the potential uses of  $\text{TiO}_2$  based-materials as photocatalyst were made by various research groups and this effort is still ongoing. Several attempts were made by researchers to investigate the potential of powdered anatase  $\text{TiO}_2$  suspension to split water. However, these experiments could not reproduce the same effect as  $\text{TiO}_2$  in electrodes. Investigation by Kawai and Sakata in 1980's concluded that the water molecules had been regenerated back by the recombination of the produced  $\text{H}_2$  and  $\text{O}_2$  in the powder system since the production sites of each gas located close to each other. To decode this dilemma, organic compound was added into the aqueous suspension of platinised  $\text{TiO}_2$  (Kawai and Sakata, 1980, Sakata and Kawai, 1981). Later, Kiwi and Grätzel (1984) also confirmed also confirmed that  $\text{H}_2$  can be produced by using anatase powder in metal dispersion. In his finding, the metal dispersion size must be less than  $10 \text{ \AA}$  to make it work efficiently. However, even though  $\text{TiO}_2$  drew many attentions due to its capability on  $\text{H}_2$  production, the biggest drawback of this material is that it can be function only under UV light irradiation. Therefore, to use  $\text{TiO}_2$  for  $\text{H}_2$  production is not a very attractive approach. Various scientist starts to look upon other semiconductor such as CdS and CdSe which has smaller band gap but their stability and efficiency are not as good as  $\text{TiO}_2$  (Frank and Bard, 1977a). Therefore, the excitement of  $\text{TiO}_2$  in  $\text{H}_2$  production research is limited in the middle of 1980's.

Conversely, the research is shifted from  $\text{H}_2$  production to decomposition of pollutant since  $\text{TiO}_2$  is also well known for its strong oxidizing power. Frank and Bard (1977b) was the pioneer to report the use of  $\text{TiO}_2$  on degrading cyanide in

aqueous suspension. Fujihira *et al.* (1981) reported on various aromatic hydrocarbons by combining the photo electrochemical production of H<sub>2</sub>O<sub>2</sub> at semiconductor electrodes with Fenton reaction. Thus, the significance potential of TiO<sub>2</sub> to detoxify pollutants in air and water is explored since nineties (Fox and Dulay, 1993, Hoffmann *et al.*, 1995).

In later years, further investigations were made by many research groups to improve TiO<sub>2</sub> performance as photocatalyst by tuning and modifying it such as through preparation method including thermal treatment or dopant introduction during the synthesis system. The manipulation of preparation method for example, allow scientist to vary many physicochemical properties of the materials by controlling the crystalline structure, surface area and particle size distribution. In 1991, Bickley and co-workers compared the photocatalytic performance of four type of TiO<sub>2</sub> specimen (P-25, pure anatase, pure rutile and mixture of anatase and rutile in proportion of 80/20) and showed that mixture of anatase and rutile (80/20) provide greater PCA compared to pure crystalline phase. Lakshmi *et al.* (1995) reported on the effect of pH on the rate of TiO<sub>2</sub> photoactivity of methylene blue (MB) under UV light illumination. The PCA was improved with increasing pH.

The importance of particles size towards TiO<sub>2</sub> photoreactivity was studied by Zhang *et al.* (1998). In their study, the photoreactivity of pure TiO<sub>2</sub> was increased as the particles size of TiO<sub>2</sub> was decreased from 21 nm to 11 nm. It is also observed that by incorporating TiO<sub>2</sub> with Fe<sup>3+</sup>, Pt and Nb<sup>5+</sup> enhanced the photocatalytic decomposition of chloroform compared to commercial Degussa P-25. Study by Burda *et al.* (2003) reported the enhancement of PCA with absorbance of visible

light region up to 600 nm by doping TiO<sub>2</sub> with nitrogen using direct amination at room temperature. However, at wavelength > 500 nm, the differences in optical response is smaller, resulting PCA under 540 nm is less pronounced. Hidalgo *et al.* (2007b) investigated the PCA activity of platinised TiO<sub>2</sub> by photodeposition method. In this study, PCA of platinised TiO<sub>2</sub> is depended on optimum size of Pt due to calcination process. Higher calcination temperature (> 500 °C) contributed toward detrimental of PCA, attributing to bigger size formation. This finding is contradicted with Lee *et al.* (2005) where they indicated that particle size of Pt did not affect the photo efficiency of TiO<sub>2</sub>.

The interest on TiO<sub>2</sub> performance as photocatalyst are still on-going, thus many scientist looking forward upgrading the functionality of TiO<sub>2</sub> to other application; antibacterial materials; self-cleaning surface, removing odors; and others (Fujishima *et al.*, 2008). Investigation by Maneerat and Hayata (2006) exhibited an antifungal activity of TiO<sub>2</sub> using in vitro and in fruit test. It is reported that TiO<sub>2</sub> in the form of powder and coated film can control the fruit sample from rot. Furthermore, it is believed that the increment of the amount of TiO<sub>2</sub> successfully suppressing *P. expansum* growth. In later year, Yaghoubi *et al.* (2010) introduced new route for TiO<sub>2</sub> coating on polycarbonate for self-cleaning materials. This method is based on wet coating using an anatase sol of TiO<sub>2</sub> nanoparticles of 30 nm size. Overall, overview on TiO<sub>2</sub> and its applications are summarized Table 2.2.

Table 2.2. An overview of TiO<sub>2</sub> research work conducted from 1970's to 2014.

| Author (Year)          | Preparation method   | Application   |
|------------------------|--|---|
| Fujishima (1972)       | Electrochemical cell using TiO <sub>2</sub> and Pt as electrodes   | H <sub>2</sub> production   |
| Frank and Bard (1977a) | Comparison of various semiconductor powder (TiO <sub>2</sub> , ZnO, CdS, Fe <sub>2</sub> O <sub>3</sub> , and WO <sub>3</sub> ) using a xenon light source | photocatalytic oxidations of CN <sup>-</sup> and SO <sup>2-</sup> |

|                                  |  |                                      |
|----------------------------------|--|--------------------------------------|
| Frank and Bard (1977b)           | Comparison of TiO <sub>2</sub> in both the anatase and rutile forms :<br>1) Undoped anatase (commercial and untreated)<br>2) Anatase + 5% rutile (treated under hydrogen gas stream at 700 °C)<br>3) Anatase + 70% rutile treated under air at 1200 °C)<br>4) Anatase from (3) + 90% rutile treated under H <sub>2</sub> at 7200 °C) | of cyanide                           |
| Kawai and Sakata (1980)          | RuO <sub>2</sub> /rutile-TiO <sub>2</sub> /Pt powdered mixture (weigh ratio= 10:100:5) was suspended in soluble carbohydrates solution (sugar or starch)   | H <sub>2</sub> production            |
| Fujihira <i>et al.</i> (1981)    | Anatase TiO <sub>2</sub> in organic suspension (Benzene, Toluene, Acetophenone)  | Photocatalytic oxidation             |
| Kiwi and Grätzel (1984)          | TiO <sub>2</sub> (P-25) was impregnated in metal suspension (Pt)   | H <sub>2</sub> production            |
| Lakshmi <i>et al.</i> (1995)     | P-25 (surface area = 50mg <sup>2</sup> g <sup>-1</sup> , mean particle size = 30 nm) in adjusting pH solution  | MB degradation                       |
| Zhang <i>et al.</i> (1998)       | 1) TiO <sub>2</sub> sol gel synthesis followed by hydrothermal (80 °C, 24 h; 180 °C, 96 h) or post calcination (450 °C, 2 h)<br>2) TiO <sub>2</sub> doped with Fe <sup>3+</sup> , Pt or Nb <sup>5+</sup>   | chloroform decomposition             |
| Burda <i>et al.</i> (2003)       | N doped TiO <sub>2</sub> using direct amination at room temperature  | MB degradation                       |
| Maneerat and Hayata (2006)       | TiO <sub>2</sub> powder (7nm) and TiO <sub>2</sub> coated film (PP film coated with 5 ml TiO <sub>2</sub> solution and dried for 72 h)   | Antibacterial ( <i>P. expansum</i> ) |
| Ashkarran <i>et al.</i> (2011)   | Ag/TiO <sub>2</sub> doped NP (Ag content = ) using sol gel and novel arc discharge method  | Rh.B degradation and antibacterial   |
| Jiao <i>et al.</i> (2012)        | Anatase – brookite nanoflower synthesized using hydrothermal method for 24 h at 180 °C   | MO and 2,4-dichlorophenol            |
| Sreethawong <i>et al.</i> (2012) | TiO <sub>2</sub> -NiO (various Ti-to-Ni molar ratios) synthesized by sol-gel process aided with laurylamine hydrochloride as structure-directing surfactant.   | MO degradation                       |
| Lin <i>et al.</i> (2014b)        | Single and co-doping of Mn and Fe in TiO <sub>2</sub> thin film using spin coating.  | MB degradation                       |
| Gharagozlou and Bayati (2014)    | Fe doped TiO <sub>2</sub> NP (Fe content from 0.01 – 0.08 g) using sol gel method and calcined at 400 °C for 4 h.  | Rh.B degradation                     |

## 2.4 Principle of the photocatalyst

The heterogeneous photocatalytic reaction is triggered when absorption of radiation is equal or greater than band-gap energies ( $E_g$ ) of the targeted

semiconductor.  $E_g$  is defined as the difference between the valence band (VB) and conduction band (CB). In the case of  $\text{TiO}_2$ , the band-gap energy for anatase and rutile are 3.2 eV and 3.0 eV, respectively. Figure 2.2 ascribed the schematic process of photogenerated electron-hole upon UV illumination. In photocatalyst system, when photon with energy equal or greater than  $E_G$  reach the particles surface, an electron ( $e^-$ ) from the valence band excited to the conduction band, leaving a hole ( $h^+$ ) behind. The photogenerated electron-hole then can recombine and dissipate the absorbed energy into heat or be available for redox reaction. The redox reaction will exploit both electron and holes, with ( $e^-$ ) for reduction process and ( $h^+$ ) for oxidation process on the  $\text{TiO}_2$  surface. Typically, the excited electron in CB will react with molecular oxygen in the air producing superoxide radical anions ( $\text{O}_2^{\bullet-}$ ) while photogenerated holes will react with water molecules forming hydroxyl radicals ( $\text{OH}^\bullet$ ) and oxidize nearby organic molecules on the  $\text{TiO}_2$  surface. The general mechanism of photocatalytic events upon light illumination is summarized in Table 2.3.

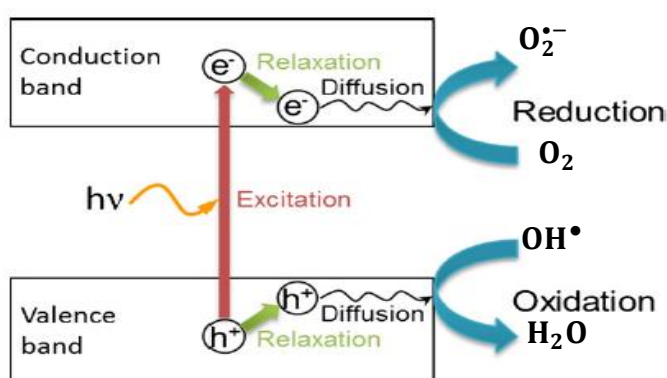


Figure 2.2. A schematic diagram for the formation of charge carriers under UV light irradiation (Nakata and Fujishima, 2012).

## 2.5 Factors that affecting PCA

### 2.5.1 Particle size

The performance of PCA in general is depended on the particle size of materials. The particle size is one of important parameters in catalysis since it affects the specific surface area and the charge carrier dynamic in semiconductor particulate. Smaller particle sizes induce the number of active surface sites and the surface charge carrier transfer rate in photocatalysis. In photocatalysis system, the photo-induced molecular reaction occurs at the surface of photocatalyst. Therefore, particle with higher surface area provides better access for reaction to take place, resulting higher yield of photocatalytic reaction. Study by Jang *et al.* (2001b) found that larger surface area could be obtained when particle size is reduced to single domain size. In order to determine their hypothesis, they conducted three set of PCA for MB, *E.coli* and ammonia gas decomposition using varied particles size of TiO<sub>2</sub>. The results revealed MB decomposition is enhanced due to particle size reduction from 30 nm to 15 nm. In addition, it is observed that 93.2% and 97.6% of *E. coli* is diminished using particle size of 30 nm and 25 nm, respectively. Similar observation also found for ammonia gas decomposition as it increased from 8% to 10% as the size of particle is reduced from 30 nm to 15 nm.

In another study, Anpo *et al.* (1987) claimed that particle size reduction changed the electronic properties of TiO<sub>2</sub> resulting to the enhancement of electron-holes activity. Zhang *et al.* (1998) reported that the PCA is increased when the particle size is reduced until it reached to an ideal size. They found that the photoreactivity of pure TiO<sub>2</sub> towards CHCl<sub>3</sub> increased when particle size is reduced from 21 to 11 nm, but decreased when the particle size further reduced to 6 nm. Xu

and Meng (2009) reported that the absorption capacity of TiO<sub>2</sub> for As(III) and As(V) increased linearly with S<sub>BET</sub> of the particles. The efficiency of As(III) photooxidation rate is clearly depended on the particle size as it decreased when particle size is increased to 30.1 nm.

To note, several literatures reported that TiO<sub>2</sub> particles with size  $\leq 10$  nm exhibits quantum size effect (Q-sized effect) (Kormann *et al.*, 1988, Choi *et al.*, 1994, Satoh *et al.*, 2008). Q-sized semiconductor such as CdS, ZnS and AgI usually shows spectral of blue-shift in absorption as consequence of exciton confinement with decreasing particle size. Although a decrease in size generally increases the band gap of semiconductors, the reported blue-shift was found to be only 0.1–0.6 eV in TiO<sub>2</sub>. In another study, Serpone *et al.* (1995) found that TiO<sub>2</sub> with particle size (2R) in the range of  $2.1 < 2R < 26.7$  nm did not show optical blue-shifts of the absorption edges. This finding is supported by Monticone *et al.* (2000) as they found that anatase with particle size 3 nm exhibits similar characteristic of bulk anatase (3.2 eV). However, when the particle size is decreased to 1 nm, they found that the absorption edge is blue-shifted about 0.1 eV from the E<sub>g</sub> of bulk anatase. This information suggested that Q-sized effects on semiconductor materials are varied from one to another depending on the type of metal oxide and their preparation method. Although Q-sized effect could enhance PCA, the disadvantage of this particular size is it requires of UV light irradiation due to wideband gap to perform PCA. However, Choi *et al.* (1994) claimed that Q-sized doped-TiO<sub>2</sub>(with metal ion) could extend the absorption band edge up to 600 nm, suggesting an enhancement of PCA under visible region.

### 2.5.2 Phase structure

Banfield (1998) reported that good crystallinity is required to reduce the formation of electron traps, which can minimize the recombination centers of photogenerated electron-holes. Several study reported that anatase exhibits the ideal PCA performance among the three crystalline phases (Ovenstone and Yanagisawa, 1999, Lee *et al.*, 2005, Adán *et al.*, 2007). Lee *et al.* (2005) found that PCA of *p*-nitrophenol is increased due to increment of anatase crystallinity in the prepared samples. On the other hand, Liu *et al.* (2008) suggested that PCA enhancement is due to the synergistic effect of crystallinity, surface area and better transmittance. Anatase prepared from peptization process at 45 to 65 °C had these three criteria which successfully enhanced PCA using Rh.B (in solution), CH<sub>3</sub>SH and HCHO (in gaseous phase) as targeted pollutants.

Another group of researchers reported that mixed phase of anatase with fraction of rutile or brookite enhanced the PCA compared to pure anatase due to electron and hole transfer between the two phases (Tian *et al.*, 2008, Kho *et al.*, 2010, Cihlar *et al.*, 2015). Kho *et al.* (2010) suggested that the mixed phase provide synergistic effect between anatase and rutile due to efficient charge separation across phase junction. Vargeese and Muralidharan (2011) observed similar behavior as anatase with small fraction of brookite (36%) synthesized using sol-gel method show high PCA using ammonium nitrate as model compound.

### 2.5.3 TiO<sub>2</sub> dosage

It is well documented that the rate and efficiency of photocatalytic would increase with catalyst loading. The increase in the efficiency seems to be attributed to

the effective surface area of catalyst and the absorption of light. At lower catalyst loading, the absorption of light controlled the photocatalytic process due to the limited catalyst surface area. However, as the catalyst loading increased, an increase in the active surface area of TiO<sub>2</sub> is obtained. The enlarged amount of photons absorbed and the amount of organic pollutants adsorbed on the TiO<sub>2</sub> surface improved the photocatalytic.

Several studies are found to support this idea. Liu *et al.* (2008) studied the effect of TiO<sub>2</sub> loading on formaldehyde under UV light irradiation for 3 h. They found that the photocatalytic reaction rate did not increase significantly when TiO<sub>2</sub> loading was higher than 2 mgcm<sup>-2</sup>. Suwarnkar *et al.* (2014) investigated the effect of Ag doped TiO<sub>2</sub> loading (0.6 to 1.4 gdm<sup>-3</sup>) on MO solution. They found that the efficiency of PCA is increased with catalyst loading from 0.6 to 1 gdm<sup>-3</sup> while loading more than that detriment the PCA. The overdosed TiO<sub>2</sub> decreased PCA is due to an increase in the particles aggregation leading to the decrease of number of active site (Sobana *et al.*, 2006). Another reason is attributed to the increment of turbidity of suspension which resulted to the inhibition of the photon absorption by the photocatalyst (Huang *et al.*, 2008).

## **2.6 TiO<sub>2</sub> synthesis**

Basically there are many methods available to produce TiO<sub>2</sub> nanoparticles such as vapor deposition, sonochemical and sol-gel method. The details of each method are reviewed in the subsequent section.